A kilowatt pulsed 94 GHz electron paramagnetic resonance spectrometer with high concentration sensitivity, high instantaneous bandwidth, and low dead time

Paul A. S. Cruickshank,[1] David R. Bolton,[1] Duncan A. Robertson,[1] Robert I. Hunter,[1] Richard J. Wylde,[2] and Graham M. Smith[1]

[1]*School of Physics and Astronomy, University of St Andrews, North Haugh, St Andrews KY16 9SS, United Kingdom*
[2]*Thomas Keating Ltd., Billingshurst, West Sussex RH14 9SH, United Kingdom*

We describe a quasioptical 94 GHz kW pulsed electron paramagnetic resonance spectrometer featuring $\pi/2$ pulses as short as 5 ns and an instantaneous bandwidth of 1 GHz in nonresonant sample holders operating in induction mode and at low temperatures. Low power pulses can be as short as 200 ps and kilowatt pulses as short as 1.5 ns with timing resolution of a few hundred picoseconds. Phase and frequency can be changed on nanosecond time scales and complex high power pulse sequences can be run at repetition rates up to 80 kHz with low dead time. We demonstrate that the combination of high power pulses at high frequencies and nonresonant cavities can offer excellent concentration sensitivity for orientation selective pulsed electron double resonance (double electron-electron resonance), where we demonstrate measurements at 1 μM concentration levels. © *2009 American Institute of Physics.* [doi:10.1063/1.3239402]

I. INTRODUCTION

The history of nuclear magnetic resonance (NMR) since the 1970s has generally been associated with the rapid evolution of sophisticated pulsed techniques and a continual push to higher fields to increase sensitivity and resolution. The development of high field pulsed electron paramagnetic resonance (EPR) or electron spin resonance (ESR) has been much slower, largely because it is much more technically challenging. Resonant frequencies at high fields are now in the millimeter-wave or submillimeter-wave region of the electromagnetic spectrum where high power amplifiers and components able to handle high powers have simply been unavailable. Typical spin relaxation times for electrons are many orders of magnitude shorter than for nuclei, and both homogeneously and inhomogeneously broadened spectra are considerably wider than their NMR counterparts; for example, a typical nitroxide spectrum extends over 500 MHz at 94 GHz (at a magnetic field of 3.35 T) and it becomes extremely difficult to excite the full spectrum with a single pulse. Limited excitation bandwidth therefore often severely limits sensitivity for many applications.

Even with partial excitation, free induction decay (FID) signals are nearly always initially swamped by the much larger transient response from the last exciting pulse and a finite time is required before any meaningful measurement can start. This is known as the *dead time* of the system and typical system dead times of 50–200 ns are often sufficiently long that the FID from many samples will decay significantly, if not completely, during this period. Fourier transform EPR or FID detection is thus relatively rare in pulsed EPR and spin echo techniques are often mandatory, usually requiring cryogenic temperatures to lengthen relaxation times and improve polarization. Even here it can be difficult to measure spin systems with short phase memory times. Ideally pulses would be created and detected on nanosecond or even subnanosecond time scales rather than the microsecond time scales common in NMR. Shorter T_1 times also mean that rapid averaging rates are required to maximize sensitivity.

Despite these challenges pulsed EPR is currently going through the same revolution that pulsed NMR experienced over 30 years ago. Cutting edge research in EPR in many areas is now dominated by the application of multidimensional, double resonance, and multifrequency pulsed techniques and there is now a push to demonstrate performance at higher magnetic fields and frequencies. Higher frequencies offer better spectral resolution, concentration and absolute sensitivity, orientation selectivity, lower cavity dead time, higher conversion factors, and access to a higher energy scale that can simplify problems associated with high energy zero-field transitions or reduce (or enhance) effects due to forbidden transitions. The past 20 years have seen a huge increase in interest in high field EPR (HFEPR) as can be seen from both general reviews of the field,[1] special editions on HFEPR,[2] and the large number of specialist reviews available, including those on inorganic systems,[3] spin labeling,[4] photosynthesis,[5] dynamics of biomolecules,[6] instrumental techniques,[7,8] quasioptical techniques,[9] transition metal ion complexes and metalloproteins,[10] instrumentation and bioinorganic systems,[11] integer spin systems,[12] molecular magnetic clusters,[13] catalysis,[14] ferromagnetic and antiferromagnetic systems,[15] relaxation,[16] and swept frequency techniques.[17] However, it is the parallel exploitation of a wide variety of pulse techniques that is revolutionizing the field (see the well known text by Schweiger and Jeschke[18]

for an excellent review). One of the main driving forces behind pulsed HFEPR has been the numerous applications in biology and recent reviews[19] and a recent book[20] have comprehensively covered developments in the field.

The first high-field pulsed EPR system was constructed by the Leiden group[21] at 94 GHz and was soon followed by systems in Moscow[22] (140 GHz), MIT (Ref. [23]) (140 GHz), and Berlin[24] (94 GHz), and in 1996 Bruker[25] introduced the first commercial pulsed *W*-band system operating at 90 GHz. Initially low source power (a few milliwatts at the cavity) limited applications for this system but in last few years the inclusion of high power solid-state amplifiers have lifted the power levels to beyond 100 mW and have allowed $\pi/2$ pulses of 30 ns duration with a dead time of 60 ns using cylindrical TE_{110} cavities. (A very recent upgrade delivers 400 mW.) High performance waveguide spectrometers operating at 94 (Ref. [26]) and 140 GHz using impact avalanche and transit time (IMPATT) amplifiers have also been described. The Frankfurt group extended pulsed EPR to 180 GHz using a combination of waveguide and quasioptical techniques and achieved 60 ns $\pi/2$ pulses for an input power of only 15 mW using a cylindrical TE_{110} resonator.[27] The Leiden group has further extended the frequency range further to 270 GHz with a remarkable fully featured TE_{110} resonator only 1.3 mm long that delivered 100 ns $\pi/2$ pulses with only 1 mW input.[28] More recently, in another remarkable feat of engineering, the Milwaukee group has constructed a miniature loop gap resonator at 94 GHz with approximately the same conversion efficiency as a high Q single mode resonator but with a Q of only 90.[29]

Most of these systems have operated at relatively low powers (1–200 mW), well within the power handling capability of standard millimeter-wave waveguide components but substantially below the pulse power levels commonly used at lower frequencies (e.g., 1 kW at 10 GHz). All the systems have featured high cavity conversion efficiencies but excitation bandwidths have nearly always been significantly smaller than in modern commercial *X*-band systems leading to substantially lower concentration sensitivity for many common measurements. There is therefore a strong motivation to operate at much higher powers at high frequencies, primarily to improve sensitivity. The value of this general approach has recently been clearly shown by the Weizmann group who incorporated a 1 W solid-state amplifier into an upgraded waveguide spectrometer at 95 GHz and demonstrated $\pi/2$ pulses of 12.5 ns, which led to significantly increased sensitivity for both pulsed electron double resonance (PELDOR) and hyperfine sublevel correlation (HYSCORE) applications.[30] Much higher powers are available from vacuum tube devices and kilowatt pulsed extended interaction klystron amplifiers (EIKAs) are commercially available at 94 GHz. However, it is still very challenging to construct systems using these devices as many critical waveguide components have difficulty in handling this level of power. Nevertheless, the Cornell group[31] has clearly shown, using quasioptical and induction mode techniques, that very high performance systems can be constructed. Using low Q Fabry–Perot resonators they have demonstrated $\pi/2$ pulses
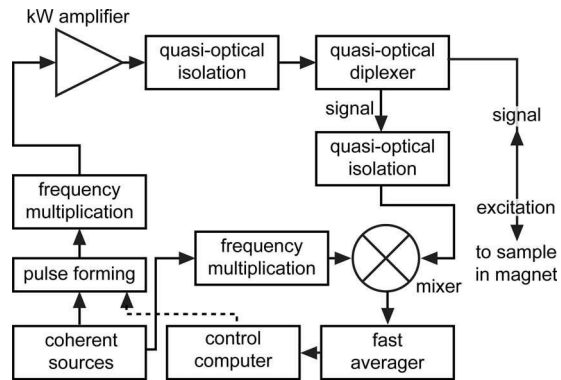

FIG. 1. Block diagram of the pulsed spectrometer showing the main elements. Most of the signal processing is done at low frequencies before multiplication and amplification. High power pulses are transmitted using quasioptical techniques to the sample and return signals duplexed to the receiver and acquisition electronics. The whole system is under computer control.

of between 4 and 6 ns, instantaneous bandwidths of 200 MHz, and dead times of 30–50 ns at room temperature.

In this paper, building on this success, we describe a spectrometer using induction mode and a similar power amplifier, but aiming to significantly improve on the flexibility and performance of the electronics, the quasioptics, and the sample holder. Our system is designed to operate at cryogenic temperatures and provide $\pi/2$ pulses as short as 5 ns on large volume samples and offers 1 GHz instantaneous bandwidth and low effective dead times. This capability can significantly improve concentration sensitivity in many critical pulsed EPR applications, while allowing relatively easy sample degassing and cold sample loading. The main design features are outlined below, followed by examples demonstrating system performance and a discussion of new opportunities.

II. DESIGN AND IMPLEMENTATION

A. System architecture

Modern pulsed EPR spectrometers are sophisticated instruments that allow the relative phase, frequency, amplitude, and timing of pulses in complex sequences to be programmed and for the resulting signals to be averaged in real time at high repetition rates. A block diagram of the whole system is shown in Fig. 1, while the transmit and receive electronics are shown in Fig. 2. The system uses a heterodyne architecture broadly similar to that described in Ref. 26, except that high power passive multipliers are used rather than IMPATT multipliers and amplifiers. This allows pulse sequences, phase cycling, and output frequencies to be defined at lower frequencies (around 7.83 GHz) using a fast data generator at up to 2.66 Gbytes/s. Two different sources may be selected on nanosecond timescales for double electron resonance experiments.

B. Pulse generation and timing

The pulses are formed at 7.833 GHz, which is obtained by up-conversion from either a phase-locked 7.683 GHz fixed-frequency dielectric resonator oscillator (DRO) (Nexyn
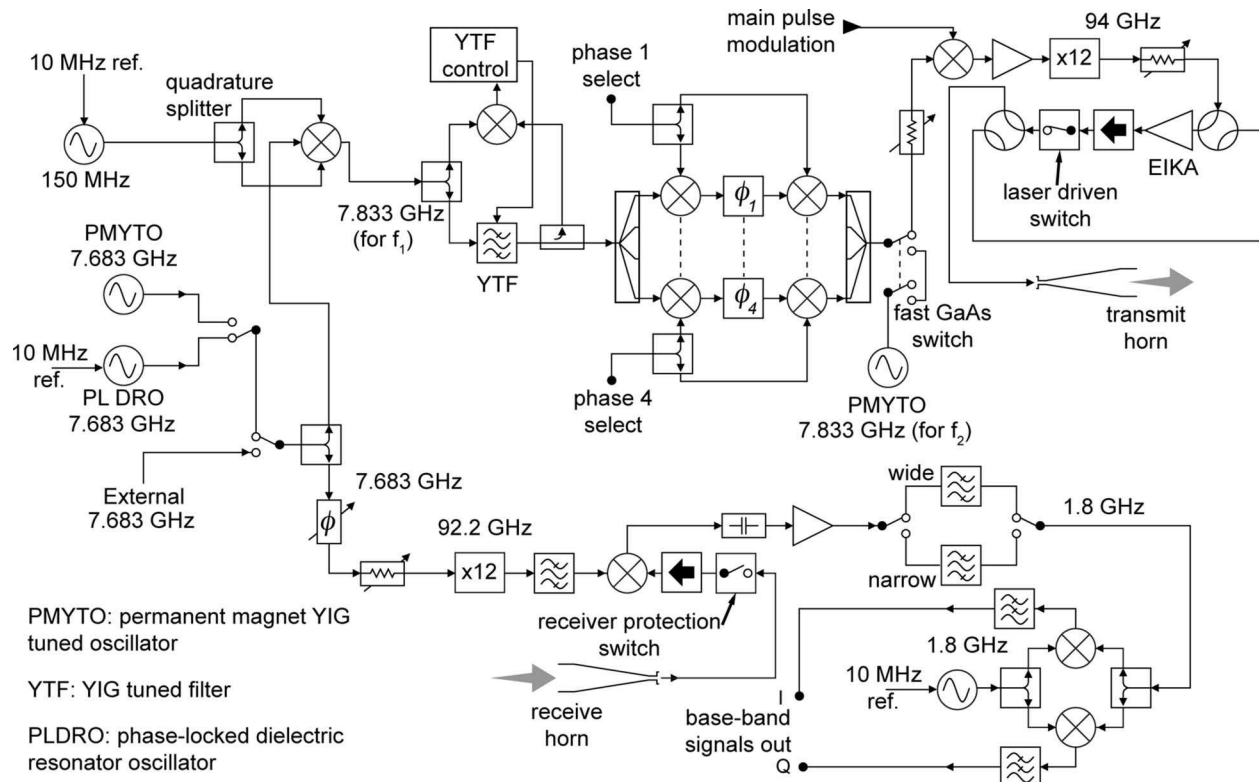
FIG. 2. Basic system diagram showing the transmit and receive electronics of the high-power EPR spectrometer. The upper part shows the transmit section and the lower part shows the receive section. The two parts are coupled through a high-performance quasioptical system.

Corp., Santa Clara, CA, USA) or from a phase-locked permanent magnet yttrium iron garget (YIG) tuned oscillator (PMYTO) (Micro Lambda Wireless, Inc., Fremont, CA, USA). The latter allows the main system frequency to be varied over the range of 93.5–94.4 GHz with only a small increase in phase noise over the DRO. The up-conversion to 7.833 GHz uses a 150 MHz crystal oscillator (Wenzel Associates, Inc., Austin, TX, USA), referenced to the system's master 10 MHz reference (also Wenzel Associates). One of four variable phase shifters may be switched in to the transmit path for each pulse to allow phase cycling.

A second PMYTO is used to provide a second transmit frequency for double resonance (e.g., PELDOR) experiments. This frequency is switched into the 7.833 GHz path after the phase cycling network using a fast GaAs switch (Hittite Microwave Corp., Chelmsford, MA, USA).

A wideband double balanced mixer (Mini-Circuits, Inc., Brooklyn, NY, USA) is used as the main pulse switch[32] with switching times of less than 300 ps at 7.833 GHz. The on-off ratio of the mixer switch is relatively poor at around 20 dB, but this is sufficient due to the properties of the following multipliers and it is preferred to a conventional switch because of the speed at which it can be modulated.

High power passive multipliers are preferred to IMPATT multipliers due to their lower noise, wider instantaneous bandwidth, and faster turnon. Our transmitter uses a ×12 chain consisting of an active tripler followed by two passive doublers (Virginia Diodes, Inc., Charlottesville, VA). This combination leads to considerable pulse sharpening over the 7.833 GHz input and produces around 200 mW at 94 GHz with effectively infinite on-off ratio pulses. This is followed

by a computer controlled rotary vane attenuator.

The switching signal for the EPR pulses is generated by the data generating component of an 81210 parametric bit error rate testing (ParBERT) system (Agilent, Inc.). This has one channel that can run at up to 2.66 Gbytes/s and eight channels that run eight times slower. The fast channel is used to drive the EPR pulse switch and the slower channels are used to drive the phase cycling switches, the second frequency select switch [for PELDOR, double electron-electron resonance (DEER), etc.], a rf switch for electron nuclear double resonance (ENDOR) experiments, and a fast pin switch for receiver protection. Further timing signals are produced via two six channel digital delay generators (Highland Technology, San Francisco, CA) to trigger other parts of the system. The overall system frequency of the ParBERT may be varied to give an EPR pulse position or length resolution from 0.33 to 2.5 ns. It is typically run with a pulse length resolution of 0.5 ns. Typical high power pulse profiles from the current system are shown in Fig. 3. The ringing observed at the leading edge of the pulse lasts for 8 ns after which the response is flat. It should be noted that this ringing is not due to the power amplifier as early testing of this amplifier (with a different preceding multiplier system) did not show this behavior.[33]

The relative delays in the system are critical to ensure that the phase cycling selection and second frequency selection pulses arrive at their targets so that the phase or frequency is not accidentally switched during a pulse. The timing for enabling the receiver is also critical to prevent damage to the receiver.
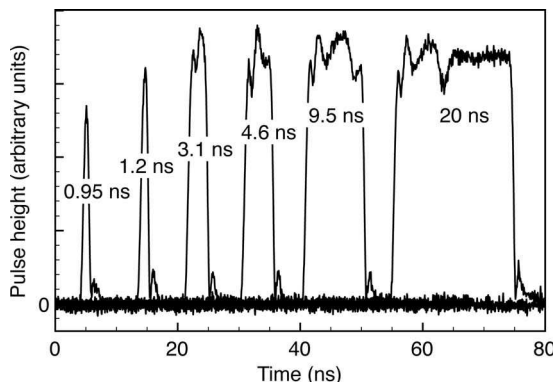
FIG. 3. High-power pulse profiles at 94 GHz as measured on a forward power monitor immediately before the input feedhorn to the quasioptical system, indicating a peak power into the optics of about 650 W. The ringing at the beginning of the pulses is systematic and after around 8 ns the pulses are very flat. The ringing is believed to be related to bandwidth limitations in the preceding electronics (and was not present in an earlier version of the system).

C. EIK amplifier

We employ a 1.3 kW pulsed EIKA, VKB2475 series, Communications and Power Industries Canada, Inc., Georgetown, ON, Canada) that offers 45 dB gain in saturation and a frequency response flat to 1.5 dB over a 1 GHz bandwidth at 94 GHz. This is followed by a high power waveguide isolator specified to handle 10 W average power (Ferrite Domen Co., St. Petersburg, Russia) required to protect the amplifier from high power accidental reflections. This limits the usable duty cycle of the EIKA to 1%, although the device itself will run at up to 10% duty. The EIKA is a compact water cooled device and may either generate relatively long pulses itself from a cw input or act to amplify input pulses.

D. Fast high power switch

Even with no input power, the EIKA produces around 1 mW of flat (white) noise across its 1 GHz bandwidth, and it takes a finite time after the final pulse to turn the device and noise off. The effect of this noise can be seen in averaged spectra at least up to 80 ns after the final pulse, which would normally significantly limit the system dead time. In *X*-band systems, this noise is often gated using high power switches, but at 94 GHz there are no commercial switches able to handle 1 kW peak powers and switch in nanoseconds. In order to minimize the effects of this noise on our measurements, an optically triggered silicon switch, based on the work of Lee *et al.*,[34] was developed which attenuates this noise by more than 30 dB, and is able to switch kilowatt power levels.[35] A schematic of this switch and its time response is shown in Fig. 4. It consists of a piece of high-resistivity silicon one wavelength (in the silicon) thick (~1 mm) placed in a single-mode split-block waveguide. The end faces of the silicon are lapped by hand until the slab is resonant in WR10 waveguide at 94 GHz. An optical fiber entering through the corner of an *H*-plane waveguide bend illuminates the face of the silicon with a single nanosecond pulse of around 20 μJ at 1064 nm from a fiber-coupled *Q*-switched Nd:yttrium vanadate laser system (Advanced Optical Technology Ltd., England). This laser can be exter-
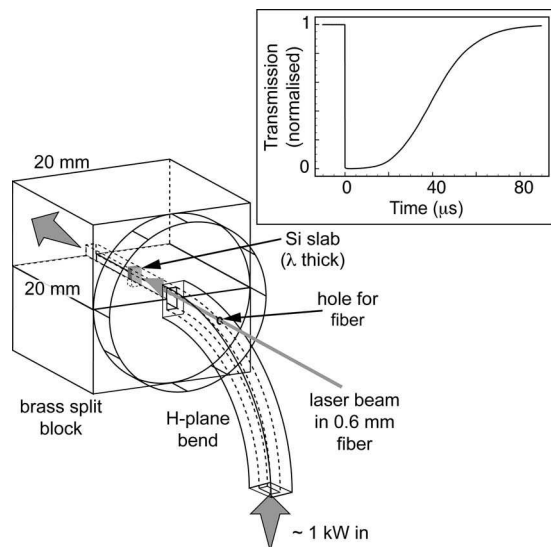

FIG. 4. The optically driven silicon switch for cutting off the EIKA noise following the last pulse. A one wavelength thick slab of high purity silicon mounted in a WR10 brass split-block waveguide is illuminated via an optical fiber, which enters through a sub-cut-off hole in the corner of an *H*-plane bend. The inset graph shows the normalized transmission at 94 GHz through the switch as a function of time after the laser pulse at time zero. The switching time is of the order of 1 ns, depending on the laser pulse length which in turn depends on the laser repetition rate.

nally triggered at up to 50 kHz with only 500 ps jitter. A high density of charge carriers is created within 1 ns to render the silicon slab reflective and very absorbing. The slab becomes transparent again in a time governed by the relaxation of the carriers in the silicon, effectively limiting the repetition frequency to below 10 kHz. The switch is very effective in reducing the noise from the amplifier to negligible levels, as can be seen by Fig. 5, which shows the effects of EIKA noise after the final pulse with the laser switched on and off.

E. Quasioptics

1. Optics

The term *quasioptics* refers to the use of optical techniques in situations where optical elements and beams have dimensions that are larger than the wavelength, but where the finite wavelength may not be ignored as with geometrical
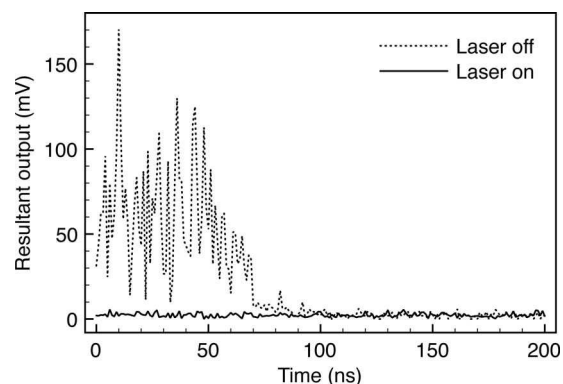

FIG. 5. Single-shot resultants of *I* and *Q* as a function of time showing the effect of the laser triggered switch in gating the dark noise. The graph starts at a point in time where the dark noise dominates over any residual ringing due to higher order modes from the probe.
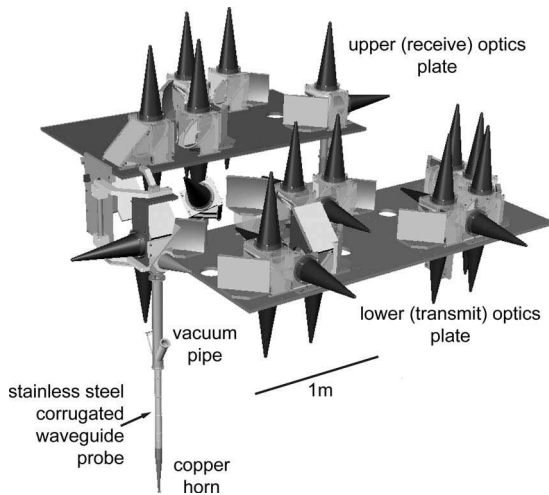
FIG. 6. 3D overview of the quasioptical system of the spectrometer. The millimeter waves enter the system through a vertical feedhorn below the far end of the lower (transmit) optics base plate and propagate through a number of quasioptical isolators before being diverted down into a stainless steel corrugated waveguide probe by the diplexer at the near end of the system. The field center of the magnet (not shown), where the sample is placed, sits 20 mm below the end of the feedhorn at the bottom of the probe. The bottom of the vacuum pipe mates with a flow cryostat inserted into the magnet to allow sample cooling.

optics.[36,37] Gaussian beam optics may be used, and the related techniques are widely applied in the millimeter- and submillimeter-wave regimes in addition to, or as an alternative to, waveguide. Here we use corrugated feedhorns[38] to transform waveguide modes to single mode optical Gaussian beams, which then are propagated in free space using off-axis mirrors through various optical components. As long as there are no major space constraints, it is the case that at 94 GHz and higher frequencies, almost every passive waveguide component has a higher performance optical analog. Our system therefore makes extensive use of these techniques to provide low loss wideband transmission, duplexing of the main signal, and very high isolation between source, sample, and detector, while reducing standing waves to an extremely low level. This is achieved through the use of very high performance feedhorns, loads, angled quasioptical isolators, wire-grid polarizers, and a large aperture corrugated waveguide.

Large off-axis reflective mirrors ($\sim 300 \times 220$ mm^2) are used to minimize stray reflections in the system and make diffractive losses negligible. The spacing and focal length of the mirrors and the size of the Gaussian beam are chosen for zero gain and frequency independent operation and so that the coma aberrations (small spatial distortions of the beam characterized by excitation of higher order optical modes) produced by one mirror are cancelled out by the aberrations produced by the following mirror.[39] A three- dimensional (3D) model of the whole system (minus the magnet) may be seen in Fig. 6.

2. Feedhorns

Corrugated feedhorns are used to transform the TE$_{10}$ waveguide mode to high purity Gaussian beam modes. The horns were designed in house using the CORRUG modeling

software (SMT Consultancies Ltd., Uxbridge, U.K.) and were manufactured by Thomas Keating Ltd., U.K. The profile of the horn is chosen to deliberately excite both the HE$_{11}$ and HE$_{12}$ modes within the horn with optimized relative amplitudes.[40] These modes are then brought into phase at the aperture and couple with extremely high efficiency (99.8%) to a fundamental Gaussian mode. This can be compared to standard scalar corrugated feedhorns, which couple with approximately 98% efficiency. Such small differences in coupling efficiency might appear unimportant, but the excitation of even small amounts of higher order modes in an over-moded system can lead to significant effects. We believe that higher order modes can contribute significantly to the ultimate cross-polar isolation that can be achieved by scattering to modes with an orthogonal polarization. Feedhorn performance was checked by measuring the far field antenna patterns, which showed significantly reduced sidelobes indicative of low higher order mode content, almost exactly in line with theoretical predictions.

3. Loads

There are many places within the system where reflections can be expected which would seriously limit the system dead time if directed back down the beamline. Examples include reflections from polarizers, Faraday rotators, and the vacuum window. The effects of these components are largely eliminated by angling them all at 45° to the beam and terminating the reflections in high quality quasioptical loads. These loads consist of 400 mm long hollow cones with a 140 mm aperture made of lossy carbon-loaded plastic. The performance is ultimately limited by multiple reflections within the cone.

The cones were injection molded and typically demonstrate 60–75 dB return loss with the cone axis parallel to the beam. A large number were made and the best selected for use in the system. Even better performance was achieved by angling the cone slightly with respect to the incoming beam where performance was below the limits of detectability (-80 to -90 dB) in our experimental setup. This compares to around 45 dB return loss for high quality planar millimeter-wave absorbers (Thomas Keating Ltd., U.K.).

4. Isolators

Of critical importance in developing systems with extremely low dead time is high isolation to prevent any standing waves between the source, detector, and sample holder. We use quasioptical Faraday rotators (QOFRs), developed in-house, between pairs of wire-grid polarizers to provide up to 60 dB peak isolation per device exactly at 94 GHz, with 0.3 dB insertion loss. These devices are temperature tuned for best performance and their design has been described in a previous paper.[41] A unit cell of our optical system including a quasioptical isolator may be seen in Fig. 7. All reflections from polarizers and rotators are terminated with quasioptical loads. Several isolators are placed in series to provide around 90 dB isolation between source and cavity and 70 dB isolation between cavity and detector across the desired 1 GHz
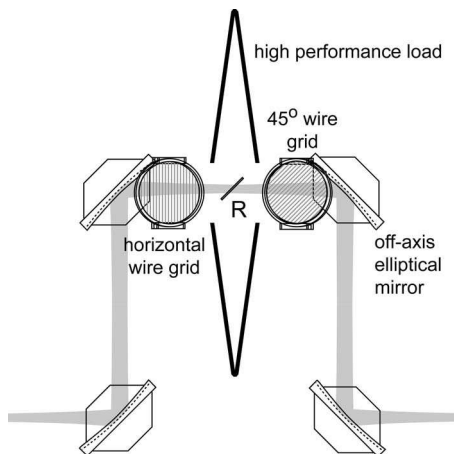
FIG. 7. A unit cell of the quasioptical system showing a single quasioptical isolator composed of two polarizing wire grids, the planes of which are at 45° to the beam direction. A signal passing through the QOFR *R* has its polarization rotated by 45° allowing it to pass through the following grid. Any returning signal is rotated by a further 45° in the same sense and is thus reflected out of the plane of the diagram by the horizontal grid. Unwanted reflections from the polarizers and *R* are terminated in the high-performance loads. Not shown are similar loads above and below each of the polarizing grids. The beam is focused from a narrow waist at *R* to subsequent narrow waists (at bottom left and right) by compensating off-axis mirror pairs which cancel out coma aberrations.
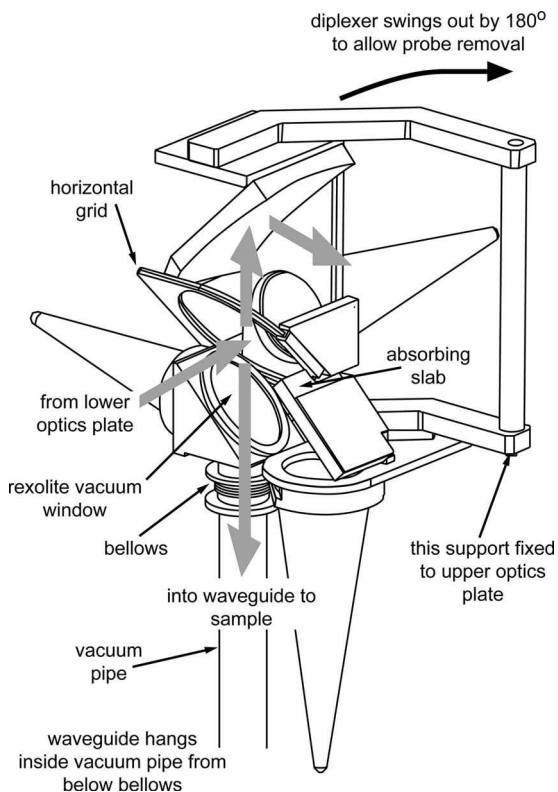

FIG. 8. The polarization based diplexer to couple to and from the sample. The excitation signal from the lower plate is reflected down through a Rexolite® vacuum window toward the sample and the majority is reflected straight back and accommodated by the quasioptical isolators in the system. The EPR signal from the sample is in the orthogonal polarization and thus passes through the grid and is directed into the receive optics. The window and loads attached to it are connected to a supporting arm that may be swung back by 180° to allow the vacuum pipe and probe to be inserted and removed from the magnet.

bandwidth: individual isolations do not simply sum due to subtleties associated with the grid orientations.

The reflection at normal incidence from a Faraday rotator is typically −25 dB and is terminated in a high performance load. Return loss from an isolator system (consisting of an angled Faraday rotator, pair of angled polarizers, and six loads) is too low to measure, but estimated to be 120 dB. This should be compared to the return loss of waveguide isolators, which is rarely better than 30 dB.

Virtually all the power incident on the sample holder is reflected back toward the source and thus the first quasioptical isolator must be capable of dumping close to 0.5 kW without reflection. This is achieved by reflecting this high power beam off a flat section of absorbing material at the Brewster angle before being directed into a load. At full power we have not been able to measure any system reflections directly associated with the optics, although there is some evidence of low level reflections related to preceding waveguide components.

5. Corrugated waveguide and vacuum window

The sample holder is in a flow cryostat at the field center of the magnet. Coupling to the sample from the optics is done via a 46 mm internal diameter, thin walled, nonmagnetic, stainless steel, cylindrical corrugated pipe.[42] Stainless steel is chosen because of its low thermal conductivity and ready availability at large diameters. Its relatively poor electrical conductivity is not a major factor because the corrugations present a high impedance to the electrical beam, which strongly limits conduction in the walls (for this size of waveguide) leading to negligible loss. The depth of the corrugations and the aperture of the guide are chosen to minimize the impedance change and reduce reflections at the aperture to negligible levels.

The flow cryostat operates in a low pressure helium environment and must be sealed from the laboratory without introducing any reflections along the beam path. The vacuum window is angled at 45° to the beam and reflections from the window are terminated in loads. The window itself is made from Rexolite® (C-lec Plastics, Inc., Willingboro, NJ), a cross-linked polystyrene which is easy to machine and has reasonably low loss at 94 GHz. The window has a 62 mm aperture and is approximately 9 mm thick to minimize distortion of the window when the cryostat is evacuated. The exact thickness is chosen to minimize reflections at 94 GHz. The vacuum window assembly itself is on a swing arm and attached to the pipe assembly via an O-ring seal that permits rotation of the entire pipe assembly. The swing arm allows the vacuum window to be rapidly removed and the probe assembly raised to allow fast cold sample loading. A schematic of the setup is shown in Fig. 8.

F. Induction mode sample holder

In strongly overcoupled systems the majority of power is directly reflected from the cavity or sample holder and at kilowatt levels would severely damage most receivers. As yet there are no commercial switches that will handle this power level at 94 GHz so it becomes critical to provide high
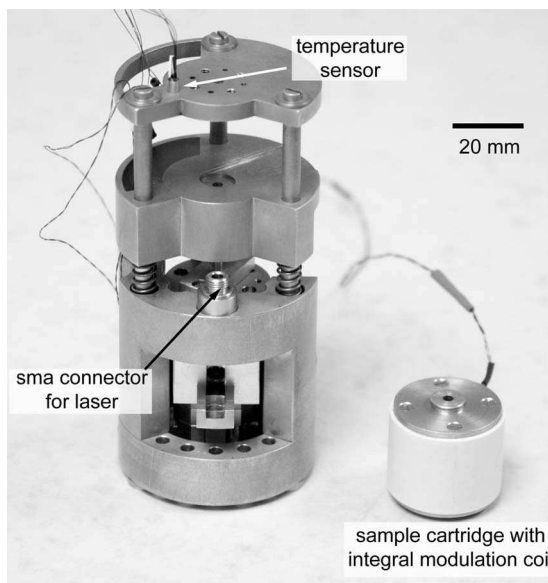
FIG. 9. A photograph of the brass sample holder together with the nickel silver and Tufset sample cartridge that allows for fast sample loading into the precooled sample holder. Different cartridges incorporate modulation coils for cw EPR and NMR coils for ENDOR and DNP, as well as the nonresonant sample holder for the sample itself.
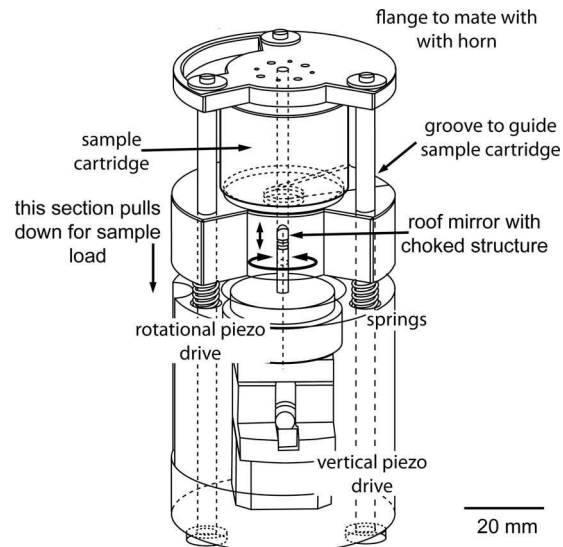

FIG. 10. Simplified cutaway sketch showing the key components of the sample holder. Underneath the sample cartridge is a roof mirror with choke structure, which may be adjusted both azimuthally and vertically by piezo-drives to cancel out stray cross-polar reflections and enhance the cross-polar performance of the system. Between the vertical and rotational drives sit miniature optics to guide a laser beam to the sample for optical excitation, but the details have been omitted for clarity.

isolation between the source and detector. This is achieved in our spectrometer by operating the cavity or sample holder in *induction* mode,[43] where the sample is excited by a linearly polarized beam, but couples power to the orthogonal mode during resonance (when a circularly polarized beam is absorbed or emitted). A wire-grid polarizer positioned directly above the vacuum window duplexes the transmit and receive signals. Both nonresonant sample holders and low Q TM_{011} cavities have been constructed that operate in induction mode and the degree of cross-polar isolation achieved when the sample is off-resonance is a critical parameter in these systems.

The current probe assembly and nonresonant sample cartridge are shown in Figs. 9 and 10. The upper part of the brass probe assembly contains a spring loaded mechanism so the sample cartridge can be rapidly inserted and locks into place. The lower part of the probe assembly has a miniature roof mirror embedded in 3 mm diameter circular waveguide in the bottom part of the mechanism that can be controlled by two piezomotors (Attocube AG, Munich, Germany) allowing the roof mirror to be independently rotated and/or moved vertically. This enables any extraneous scattering of the input pulses into the cross polarization by the sample (or probe) to be interferometrically cancelled by adjusting the mirror position. Using this technique, we typically achieve 45 dB isolation, while isolations of 60 dB have been demonstrated (over narrow bandwidths). Good cross polar isolation is important to protect the receiver from the high power excitation and reduce the effects of phase noise (for cw applications) and amplifier dark noise (for pulsed measurements). The probe assembly also incorporates optics to allow light excitation of the sample. The sample cartridge consists of a central 3 mm diameter circular waveguide in which a 3 mm diameter quartz tube up to 25 mm long can be seated, housed in a nickel silver and Tufset$^{®}$ (Tufnol Composites Ltd., Bir-

mingham, U.K.) block. Several cartridges are available and can contain modulation coils for cw measurements as well as coils for ENDOR or NMR.

G. Magnet

The magnet is a 9 T superconducting system (Magnex Scientific Ltd., Oxford, U.K.) with a 89 mm room temperature bore. The magnet has permanent leads but is fitted with a persistent mode switch and incorporates a nonpersistent ± 0.2 T superconducting sweep coil. The static liquid helium consumption is around 2.5 l per day. Separate power supplies (both IPS 120, Oxford Instruments Ltd., Abingdon, U.K.) drive the main and sweep coils in the magnet and the sweep coil power supply is under computer control.

A 62 mm internal diameter continuous flow cryostat (SpectronNMR 62, Oxford Instruments) is used to control the sample temperature using an Oxford Instruments ITC 503 temperature controller under computer control. The temperature near the sample, as opposed to the cryostat heat exchanger, is separately monitored.

H. Receiver system

The basic system layout for the receiver system is shown in the lower part of Fig. 2. A fast PIN switch (rise time of ~1.6 ns) (ELVA-1, Riga, Latvia) is used to protect the receiver. It can accommodate a peak power of up to 5 W, depending on pulse length and duty cycle. An isolator between the switch and the front end mixer prevents LO leakage from the mixer causing a large IF transient when the PIN switch changes state. The mixer is part of a down conversion unit consisting of a ×12 multiplier (from the 7.683 GHz drive to give the 92.2 GHz LO) and a waveguide filter (Millitech, Inc., USA). This is followed by a dc block and an IF amplifier before either a 1 GHz Gaussian bandpass filter
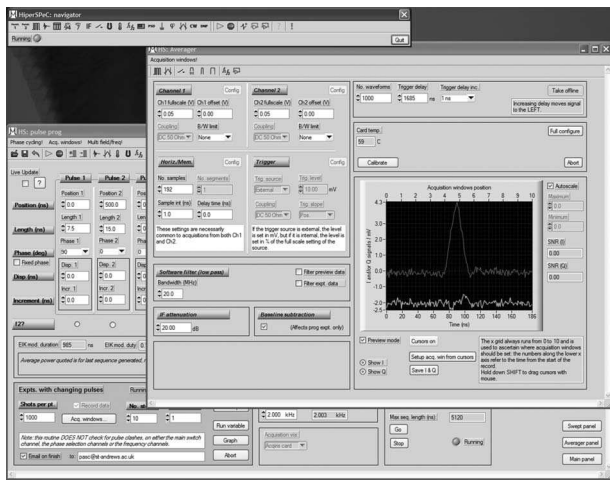
FIG. 11. A screen shot of the home-written user interface used to operate the spectrometer. The controls for different aspects of the system are spread across many panels which may be displayed or hidden at will: those shown are for programming the pulse sequences, configuring the acquisition and navigating through all the other available panels.

(used for pulsed operation) or a 30 MHz bandpass filter (used for cw operation). A further amplifier in conjunction with a computer controlled attenuator allows for optimum gain setting. The 1.8 GHz IF signal is then mixed down to base band in an IQ demodulator, the reference of which is locked to the system 10 MHz master clock or derived from the 150 MHz interpolation oscillator. The I and Q outputs are further filtered to remove any 1.8 GHz leakage. The LO path at 7.683 GHz incorporates a delay line to equalize the LO and signal paths and reduce the effects of phase noise on cw measurements. The system noise temperature at the input of the mixer was measured to be 1200 K.

I. System control and data acquisition

The whole instrument is controlled from an industrial, rack-mounted personal computer running WINDOWS XP and using software written in National Instruments' LABWINDOWS/CVI to control the pulse generation, data acquisition, and all the ancillary instruments used in the spectrometer. LABWINDOWS/CVI is an environment for developing virtual instrumentation using ANSI C, offering the advantages of C together with extensive support for instrumentation control. Switches and level-set attenuators are controlled via a homemade parallel bus driven from a digital output card. Safety of key components is a principal concern so the EIKA is interlocked such that it will only operate if the movable arm of the optics (see Fig. 8) is locked in position and the high-power waveguide path is selected.

The software has been developed to allow intuitive control over complex pulse sequences and multiple automated runs for long experiments. Sequences of up to eight pulses that may include moving and changing the lengths of multiple pulses are constructed using a graphical user interface, illustrated in Fig. 11, and multiple runs may be averaged together. The software could easily be adapted to allow sequences containing more pulses. The user may also specify up to eight combinations of magnetic field and the frequencies of both available oscillators to automatically acquire

large data sets, e.g., for orientation selective PELDOR. Tables of phase values are simply constructed in the UI for phase cycling.

The EPR signal is captured using a two channel, 1 GSa/s per channel fast PCI averager (Agilent Acqiris AP240 U1082A-AVG). Both 8 bit channels have 1 GHz analog bandwidth and the card can average up to 65 535 acquired waveforms in real time before reading the final (up to 24 bits deep) result out. The card can acquire at repetition rates above 1 MHz, much faster than the 85 kHz limit imposed on the repetition rate by the EIKA. After acquisition of the averaged waveforms, the signal is integrated over user specified limits.

III. SYSTEM PERFORMANCE

A. Typical $\pi/2$ pulse lengths

Nonresonant sample holders have relatively poor B_1 homogeneity over the volume of the sample and so the $\pi/2$ pulse length should be understood as an average over the entire sample and is defined as the "pulse length that gives the largest signal" in standard FID or spin echo measurements. In practice, there will be parts of the sample that will experience considerably higher or lower B_1 fields than indicated by the nominal $\pi/2$ pulse length. With samples contained in 3 mm o.d./2.5 mm i.d. quartz tubes positioned within 3 mm circular waveguide, $\pi/2$ lengths have varied from 4 to 10 ns depending on sample and temperature. A $\pi/2$ length of 6.5 ns is routinely achieved in our nonresonant sample holder for frozen biological samples in water/glycerol corresponding to a conversion factor, referenced to the input power at the transmit horn, of 0.6 G/W$^{1/2}$. A modest increase in conversion factor is expected for smaller radii waveguides until cutoff is approached, where the longitudinal waveguide B_1 component increases at the expense of the transverse waveguide B_1 component. On the other hand, by increasing the radius of the sample holder the sample volume will increase faster than the conversion factor falls, so for pulse methodologies that do not require high excitation bandwidths (such as Davies ENDOR), concentration sensitivity can potentially be increased by increasing sample volume.

Higher conversion factors are, of course, available with cavities and we have constructed and tested a miniature TM$_{110}$ cavity, also operating in induction mode, and in preliminary experiments we have achieved $\pi/2$ pulses of just over 2 ns, as indicated in the nutation data, shown in Fig. 12. This cavity had a Q of 200–300 (which is larger than ideal for a 2 ns pulse) and a diameter of $\sim$3 mm and the sample was contained in a 0.3 mm i.d. quartz tube with an effective length of 2 mm. At present, the increase in conversion factor is more than outweighed by the significant reduction in sample volume leading to a significant loss in concentration sensitivity for nonlossy samples. It is also more difficult to optimize the cross-polar isolation. However, we believe this is the shortest $\pi/2$ pulse reported for a high-field EPR spectrometer and the cavity also has the advantage that it can be used with aqueous samples without significantly affecting the Q.
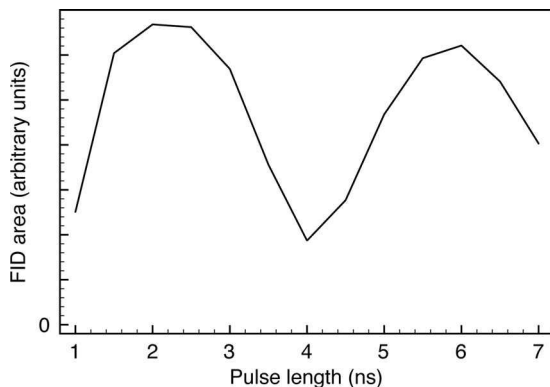
FIG. 12. Nutation experiment showing the magnitude of the FID response from a small sample of fluoranthene in a TM_{110} cavity as a function of pulse length.

B. Power handling

The 94 GHz EIKA is capable of peak powers in excess of 1 kW and average powers of over 100 W. In general, high peak power can be expected to cause problems with dielectric breakdown while high average power can cause problems with thermal loading. Dielectric breakdown is expected to occur at powers above 5 kW in single-mode waveguide at 94 GHz and at somewhat lower powers in low pressure helium environments, and is expected to be an issue in high Q cavities and for any solid-state device such as *pin* diodes or Schottky diode mixers where local E-fields will be high. In general, however, high average power levels are much more of a problem. In tests, both the Faraday rotators and the loads started to show damage for an average input power of several tens of watts. The high power waveguide isolator used to protect the EIKA from reflections has a maximum average power rating of 10 W. Therefore the maximum duty cycle is software limited to only permit pulse sequences that have an average power of less than a few watts, and this rarely imposes any limitation on desired pulse sequences. It might be thought that even these power levels could cause problems for biological samples. However, while this might be true for aqueous samples, in practice dielectric losses for most materials become rather small at cryogenic temperatures and we have seen little evidence of thermal absorption even at high repetition rates. We have demonstrated high quality field swept echo measurements at a repetition rate of 72 kHz on water/glycerol biological samples at 10 K with 4 ns $\pi/2$ pulses and 8 ns π pulses, where the temperature monitored near the sample remained constant to within 0.01 K over extended periods. With the exception of strongly polar (high loss) solvents at room temperature and very high concentration samples, power handling associated with sample losses has not yet been a major issue.

C. Sample handling

One of the most important practical aspects associated with high frequency EPR is sample handling and sample preparation, including degassing and efficient loading at low temperatures. This is often difficult using conventional 0.6 mm internal diameter tubes often used at W-band with cylindrical resonators. However the 2.5 mm i.d. quartz tube used in our nonresonant system is large enough to allow straightforward sample handling, sample degassing, and preparation of good glassy samples. For cold sample loading both cartridge and sample are precooled in liquid nitrogen and the probe assembly is precooled in the flow cryostat to typically 100 K. The flow cryostat is then brought up to atmospheric pressure with helium before the duplexer is swung back on its arm. The probe assembly is then rapidly removed with the aid of a small hoist and the sample cartridge inserted via a spring loaded mechanism, connectors attached, and the whole assembly lowered back into the flow cryostat and a vacuum reestablished with the duplexer back in place. The typical time for loading a sample is less than a minute, from stopping the helium flow pump before opening the cryostat to starting it again after loading the sample and replacing the probe. This approach has allowed routine cold sample loading, which is often important for biological samples.

D. Dead time

There can be a large number of contributions to dead time at high frequencies and these have been discussed extensively by Freed and co-workers,[31,44] and more recently by Smith *et al.*[8] They include cavity ringdown, system reflections, amplifier noise, detector recovery, and the length of the exciting $\pi/2$ pulse itself. Each of these, under certain circumstances, may contribute to dead times of the order of 100 ns. Many of these contributions are significantly reduced by the high cross-polar isolation in our system achieved with induction mode. Cavity ringdown often dominates dead time at lower frequencies where cavities are large, but a nonresonant system, even allowing for reflections within the sample, is expected to allow power in the sample holder to decay to thermal noise within 1 ns. Standing waves in the system are expected to be more troublesome at high frequencies where path lengths can be long,[31] so great care has been taken to eliminate such effects, and we have found no evidence that standing waves contribute significantly to our dead time. The use of a fast PIN switch before the detector keeps the power at the receiver low enough to ensure negligible dead time associated with recovery from receiver saturation. The combination of the laser switch and high cross-polar isolation reduces the dark noise from the amplifier to below the detector noise level (see Fig. 5). A short transient signal lasting a few nanoseconds is observed in the output of the EIKA (see Fig. 3), and its effect is significantly attenuated, but not eliminated, by the laser switch and the cross-polar isolation. However, we believe that the most significant contribution to dead time in our system is a very subtle effect related to higher order mode generation inside the corrugated feedhorn transition immediately above the probe assembly. Some of these higher order modes appear to have sufficiently high cross-polar components, and sufficiently low group velocity in the corrugated waveguide relative to the main pulse, that they can appear to arrive at the detector as long as tens of nanoseconds after the final pulse. These additional spurious responses cannot be "tuned out" with the roof mirror in the sample holder and are sensitive to small variations in the positioning of the whole corrugated pipe assembly but their magnitude is significantly reduced by replacing the horn at
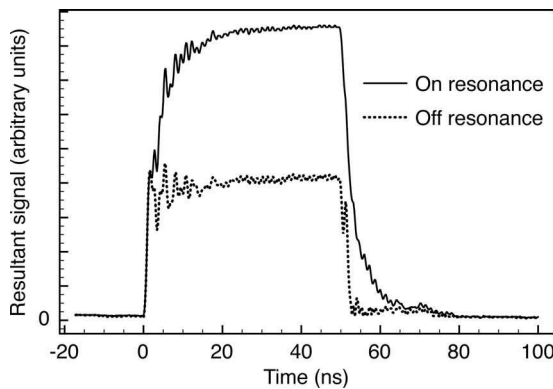
FIG. 13. The FID from a large DPPH sample with the receiver enabled during a small turning angle (low power) of 50 ns pulse showing the signal buildup during the pulse as well as the FID following the end of the pulse. Both lines show the resultant of the receiver I and Q outputs: the broken line when the magnet field is off-resonance and the solid line on-resonance. The cross-polar isolation required for this measurement was around 60 dB.
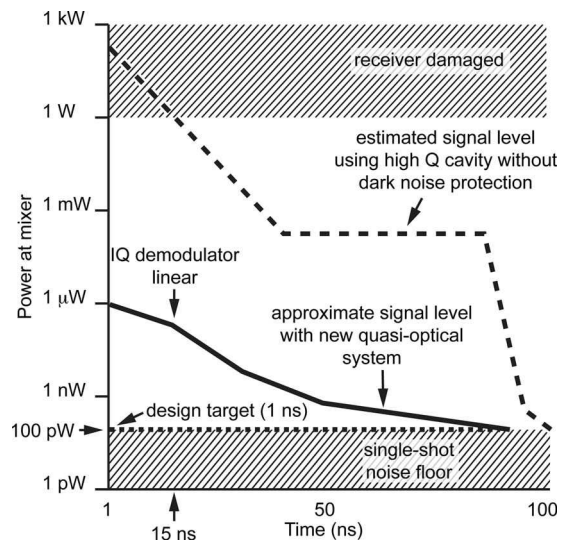

FIG. 14. Diagram indicating schematically the estimated envelope of the peak transient power at the front-end mixer as a function of time after the end of the last kilowatt pulse for our system. For comparison, the upper line shows the minimum expected transient response that could be expected from a "traditional" high-Q cavity system ($Q=1500$) with no dark-noise protection.

the bottom of the corrugated pipe with a flat reflecting plate. It should be stressed that these effects appear at a very low level (<60 dBc) and would be unimportant for almost any other application. We are about to replace the feedhorn with a modified design in an attempt to reduce these effects. We also often see transient "spikes," several decibels above the main pulse, at the beginning and end of each pulse and lasting for 2 or 3 ns, and believe these to be linked to the broad band of frequencies associated with the very fast pulse edges and the limited bandwidth of the (very high) cross-polar isolation.

The length of the excitation pulse itself can also be a significant contributor to dead time. In this context it is worth noting that the strength of the FID signal and the coherent spurious signals both scale with input power (until the $\pi/2$ pulse length is reached). Therefore, if the dominant source of noise/interference is due to transient decay of pulses, there is no advantage to operating at high power levels for FID measurements (although this is not true for spin echo measurements). This means that for very strong signals, low power (low turning angle) FID measurements can be made during the pulse itself with zero effective dead time. This is illustrated in Fig. 13, which shows the transient on-resonance resultant response from a sample of diphenylpicryl-hydrazyl (DPPH) *during* a 50 ns exciting pulse (with the receiver enabled the whole time), with the off-resonance resultant showing just the signal from the exciting pulse for comparison. This result was obtained with 40 mW input power and 60 dB of cross-polar isolation. It should be noted that the spectral width of this particular DPPH sample (Aldrich) is considerably larger at W-band than at lower frequencies. This broadening at high fields has been previously reported by several groups[45] and has been attributed to g-anisotropy. The FID signal decays over a surprisingly short time scale and would not be observable by conventional spectrometers.

In general, rather than specify a single dead time, a more useful metric is the spurious signal level both during and after the pulse. This is indicated schematically in Fig. 14, which indicates the envelope of a typical peak spurious response at the detector as a function of time after the end of a

high-power pulse. The receiver is no longer fully saturated at 1 ns after the end of the pulse and is well within its linear region after 15 ns. This is limited by the dynamic range of the IQ demodulator, which is currently being upgraded for an estimated extra 15 dB in dynamic range. Also shown, for comparison, is the expected minimum interference level from cavity ringing and amplifier noise if the nonresonant induction mode "cavity" were replaced by a traditional system with a single-mode cavity with a Q of 1500. It should be noted the exact spurious signal level depends on the precise positioning and alignment of the waveguide and probe assembly and we have previously achieved 10 ns dead time, defined as the time before spurious signals fall to the single shot noise level.

We believe the dead-time performance detailed above represents a significant advance on the state of the art for pulsed EPR and allows several new measurement protocols to be investigated, particularly for high concentration samples with short relaxation times. However, it should also be stressed that it is still above the level required to make FID detection a routine measurement in EPR and work is continuing to improve performance further.

E. Continuous-wave sensitivity

For samples that do not saturate, single-mode cylindrical resonators should offer higher cw concentration sensitivity and very much higher absolute sensitivity than nonresonant sample holders for the same input power. However, in practice, the useful maximum input power to cavities is limited either by saturation effects or issues related to phase noise on the source and its conversion to amplitude noise in high Q cavities. This is particularly important at high fields because phase noise intrinsically increases with frequency, whether using a fundamental oscillator or from a multiplied source. In these cases, nonresonant sample holders operating in in-
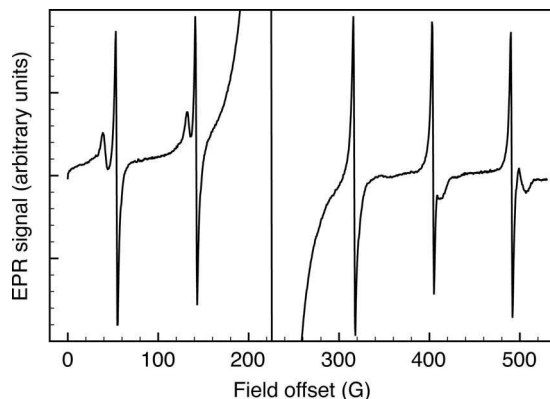
FIG. 15. A cw spectrum of 0.003% Mn^{2+} in MgO taken with a 300 ms time constant showing the high continuous-wave sensitivity of the spectrometer. The central peak due to an oxygen vacancy in MgO has been truncated to show the manganese lines more clearly.

FIG. 16. (a) A field swept echo of a 1.9 nm biradical model system in deuterated orthoterphenyl at 57 K at 1 μM concentration at 94 GHz using a nonresonant sample holder and 9 ns-τ-18 ns pulse sequence. (b) The same measurement carried out under similar conditions on a Bruker Elexys 580 pulsed X-band spectrometer using an MD4 cavity and 16 ns-τ-32 ns pulse sequence. As well as the expected improvement in spectral resolution due to the higher field, the signal-to-noise ratio is estimated to be 7 and 8 times better.

duction mode can often give higher concentration sensitivity as significantly more power can be applied before encountering the limitations mentioned above. Sample handling is also much easier, and effects related to unwanted impurity signals at low temperatures are also reduced as they are not enhanced by a high Q. Figure 15 shows a spectrum of 0.003% Mn^{2+} in MgO of a test sample that has previously been used as a concentration standard between European HFEPR laboratories. The large central line is believed to be associated with an oxygen vacancy. Direct comparisons with measurements from modern commercial cw W-band systems using high Q single-mode cylindrical cavities have shown comparable or higher sensitivity using the nonresonant system for the same modulation and time constant parameters.

F. Pulsed sensitivity

Models for cw sensitivity are well established in EPR, but the situation in pulsed EPR is much more complex and depends on the details of the pulse sequence and available power. Expressions for sensitivity for pulsed EPR have been discussed in a number of sources.[44,46] For the same type of cavity, assuming constant cavity bandwidth, the conversion factor c is expected to scale roughly with $\omega_0^{3/2}$ and the sample volume is expected to scale with ω_0^{-3}. Where the sample volume V_s is fixed, the absolute sensitivity is expected to scale as $\omega_0^{7/2}$. Thus if power is limited, cylindrical cavities are an optimum choice at high fields where they offer the best absolute (point sample) sensitivity combined with moderately high bandwidths. However, if sample volume is not limited, the concentration sensitivity is only expected to scale as $\omega_0^{1/2}$ and there appears to be little hope for dramatic improvements by further increasing the frequency, as there is inevitably an increase in the system noise figure. However, if power is not limited (for the desired excitation bandwidth) and sample losses are relatively low it is nearly always possible to increase sample volume V_s, at the cost of reduced conversion factor c, but still increase concentration sensitivity. In a comparison of commercial X-band cavities, Höfer and Carl[47] showed that a large volume Bruker MD5 or MD4 cavity has five times the concentration sensitivity of the smaller volume MS2 cavity, while having three times less
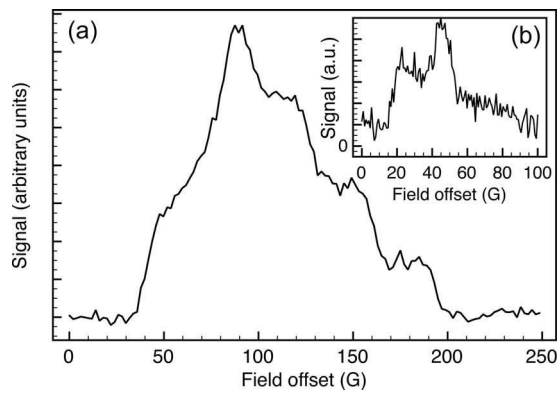
absolute sensitivity. In the limiting case, a natural extrapolation to higher sample volumes leads to the nonresonant sample holder. It is a fundamental insight in this paper that, for many samples, losses at W-band can remain sufficiently low for this scheme to be used to significantly improve concentration sensitivity for pulsed EPR at W-band, while offering extremely large instantaneous bandwidths, negligible cavity dead times, and simpler sample handling.

We have previously suggested[8] a figure of merit $F = c\omega_0^2 V_s$ to allow better comparisons between different cavities or nonresonant sample holders at different frequencies, where c is the effective conversion factor of the cavity or sample holder and V_s is understood to be an effective volume allowing for B_1 inhomogeneity over the sample. Importantly this expression assumes that the system is not power limited and that it is possible to fully excite the desired spectrum, which is an important limitation at high fields. Using this measure, more than an order of magnitude improvement in concentration sensitivity is predicted relative to a MD4 cavity at X-band (for cavity settings typically used for high sensitivity PELDOR measurements). Figure 16 shows a comparative set of field swept echo measurements on a model of 1.95 nm biradical system (radical 6•• in Ref. 48) in deuterated orthoterphenyl at 57 K at 1 μM concentration at 94 GHz using a nonresonant sample holder and a 9 ns-τ-18 ns pulse sequence and 1000 shots per point. For comparison the same measurement was carried out under similar conditions on a Bruker Elexys 580 pulsed X-band spectrometer using an MD4 cavity and 16 ns-τ-32 ns pulse sequence and 1000 shots per point (using a cavity Q optimized for PELDOR measurements). A further increase in sensitivity of around 4 dB at W-band might be anticipated by improving the system noise figure by replacing the isolator, before the front-end mixer, by a low noise amplifier at the cost of lowering the damage threshold and dynamic range. Significant increases in concentration sensitivity can be expected to be important for a whole range of pulsed EPR measurements, particularly those that currently involve long averaging times—for ex-
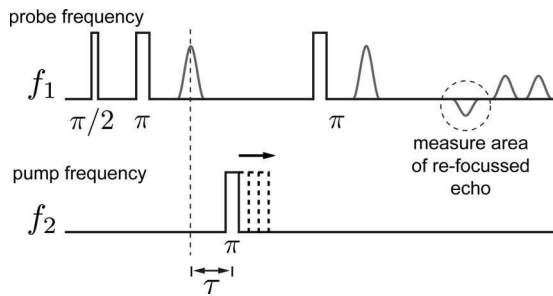
FIG. 17. The pulse sequence used in a four pulse PELDOR (DEER) experiment consisting of a three pulse probe sequence at frequency f_1, which is modulated by an inverting pump pulse at frequency f_2. The refocused echo (highlighted) is modulated as the position of the pump pulse is varied in time.
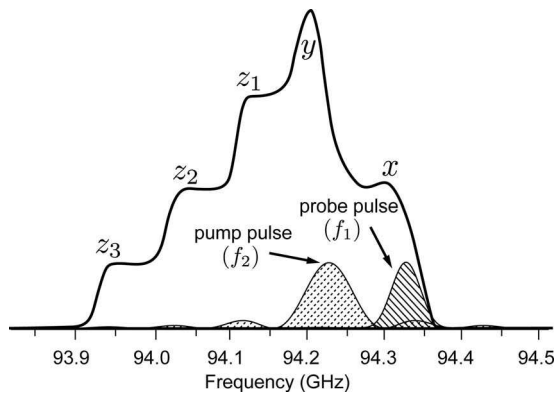

FIG. 18. A schematic frequency spectrum of a nitroxide radical showing typical excitation bandwidths of the probe and pump pulses for an orientation dependent PELDOR (DEER) experiment, although the pulses could be positioned anywhere across the line. Note that as the axis is in terms of frequency rather than field, the spectrum appears "backward." The excitation bandwidths shown assume probe pulse widths of 6, 12, and 12 ns and a pump pulse width of 12 ns.

ample, the popular PELDOR measurements discussed below.

G. PELDOR sensitivity

One of the most important pulsed EPR methodologies is PELDOR, also known as DEER, when used in conjunction with site directed spin labeling[49] to measure long distances in biomolecules.[50,51] The most common PELDOR pulse sequence used today is the four pulse sequence pioneered by Jeschke and co-workers,[52] shown in Fig. 17. This features a three pulse refocused spin echo sequence at a probe frequency f_1, whose echo is modulated by varying the timing τ, relative to the first refocused echo, of a π pump pulse at frequency f_2, which flips spins that are dipolar coupled to the probe spins. As the time τ is varied, the echo size $V(\tau)$ varies as

$$V(\tau) = V_{\text{inter}}(\tau) V_{\text{intra}}(\tau), \tag{1}$$

where

$$V_{\text{intra}}(\tau) = 1 - \int_0^{\pi/2} \lambda(\theta)\{1 - \cos[\omega_{dd}(3\cos^2\theta - 1)\tau]\}\sin\theta d\theta \tag{2}$$

represents the intramolecular dipolar interaction between the spin pair, r is the distance between the spins, and θ is the angle between the magnetic field and the vector connecting the spins. $\lambda(\theta)$ is the modulation depth parameter (the relative change in echo signal as a function of pump pulse position, which becomes angle dependent at high fields) and ω_{dd} is the dipolar coupling constant, which has a $1/r^3$ dependence. $V_{\text{inter}}(t)$, given by

$$V_{\text{inter}}(\tau) = \exp(-kCF_{\text{pump}}\tau), \tag{3}$$

represents the effects of the intermolecular dipolar interactions from all the other spins and is dependent on the concentration C of the spins and the fraction F_{pump} of spins that are excited by the pump pulse. k is a constant. At X-band, the input pulses excite essentially all orientations and distances, and distance distributions can be derived from fitting the time response (see Ref. 51 and references therein). However, at W-band and higher frequencies the g-anisotropy is sufficiently large to make the measurement orientation selective and the input pulses will now excite particular orientations of spins, as indicated in Fig. 18, and λ becomes angle depen-

dent. In principle, a series of PELDOR measurements for different pump and probe positions across the spectrum should allow the relative angular distributions of the spins to be derived. More importantly, it ought to be possible to characterize a net change in the relative orientation between pairs of spins (by measuring changes in λ), even in the presence of large distance distributions, often found in biological samples. This may prove to be a powerful tool in characterizing conformational changes, where angular movements between domains are a common biomolecular motif.

High field orientation dependent PELDOR has already been demonstrated by Bennati *et al.*[53] at 180 GHz using a homebuilt system[54] and at 94 GHz by Jeschke and co-workers[55] using a commercial *W*-band system. However, both these measurements were made at relatively low powers which limited the excitation bandwidths of both the pump and probe, thereby limiting sensitivity, and used high Q cavities, which limited the spectral separation of pump and probe, making it possible only to examine interactions between sets of spins with virtually the same orientation.

In the system described here, with nonresonant sample holders, it is possible to have near optimal excitation bandwidths (~12 ns π pulses for both pump and probe) where the relatively large sample volume more than compensates for any loss of signal due to lack of Q. The 1 GHz instantaneous bandwidth allows both pump and probe pulses to be positioned anywhere within the 500 MHz spectral width of the nitroxide spectrum, allowing any spin orientation to be correlated against any other by measuring the modulation depth. This is a measure of the fraction of spins coupled to the probe spins that have been excited by the pump pulse for that molecular orientation. In practice, a set of six pump probe PELDOR measurements is made correlating XY, YZ, XZ, XX, YY, and ZZ. Figure 19 shows an illustrative set of measurements on the same model of 1.95 nm biradical system[53] mentioned above in deuterated orthoterphenyl at room temperature at a repetition rate of 50 kHz. Each measurement took around 25 min.

Initial measurements on a variety of model and biomo-
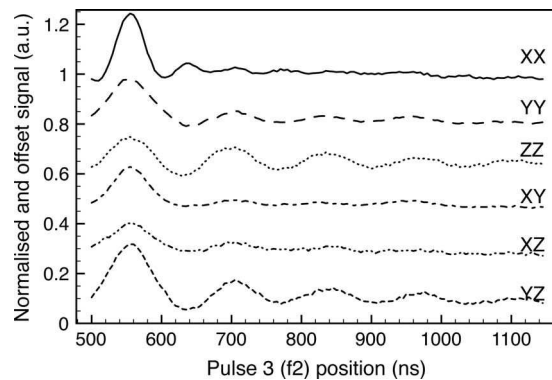
FIG. 19. Time traces of four-pulse PELDOR experiments on a model of 1.9 nm biradical system in deuterated orthoterphenyl at 100 μM concentration at 94 GHz at room temperature, correlating different orientations between spins. The first letter in each label denotes the portion of the spectrum which was pumped (i.e., corresponding to f_2) and the second letter of the label denotes the position in the spectrum which was probed (corresponding to f_1). f_1 in all cases was 94 GHz with the magnetic field and f_2 adjusted appropriately. The excellent signal-to-noise ratio at room temperature is made possible by the short T_1 of the sample allowing high repetition rates. Each trace, the average of five scans with 65 535 shots per data point and a shot repetition rate of 50 kHz, took around 25 min to acquire. The frequency separations (f_2-f_1) for the different traces were as follows: *XX*: −98 GHz; *YY*: −98 MHz; *ZZ*: 56 MHz; *YZ*: 179 MHz; *XZ*: 255 MHz; and *XY*: 76 MHz.

lecular systems have shown significantly improved concentration sensitivity relative to current *X* and *W*-band commercial cavity based systems. As an example, Fig. 20 shows a PELDOR measurement of the same system as in Fig. 16 at 57 K at a molecular concentration of only 1 μM (2 μM spins). This four-pulse PELDOR measurement took 8 h and used a 9 ns $\pi/2$ pulse and 18 ns π pulses for the probe and an 18 ns π pulse for the pump. We have not found it possible to make practical PELDOR measurements at *X*-band on this sample using a Bruker E580 system with an MD4 cavity. We are also not aware of any practical PELDOR measurements in the literature at this level of sample concentration. This measurement is also consistent with our general observation of improvements in PELDOR concentration sensitivity of
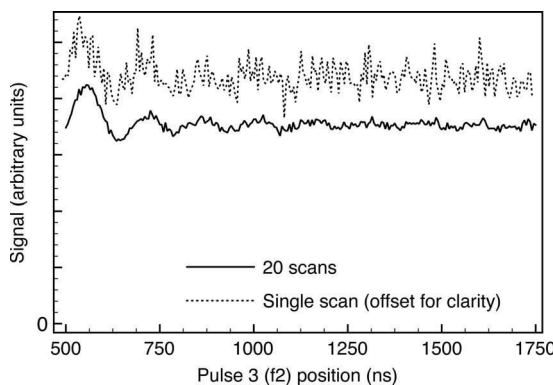

FIG. 20. A four pulse PELDOR (DEER) measurement on a model of 1.9 nm biradical system in toluene at 57 K at 1 μM concentration at 94 GHz (f_1) using a nonresonant sample holder and a 9, 18, and 18 ns probe pulse sequence with an 18 ns pump pulse. The lower trace shows the average of 20 scans of around 23 min each and the upper trace is a single scan from the same run, offset for clarity. The modulation is clearly visible in a single scan. Each scan used 1000 shots per data point at a repetition rate of 250 Hz. The frequency separation (f_2-f_1) was 98 MHz.

factors of 7 and 8 compared to our *X*-band system for a number of model and biological samples (when pumping on *Y* and probing on *X* and using the same time window). This leads to a reduction in averaging times by a factor of more than 50. In these comparisons, our *X*-band PELDOR setup has been optimized over many years in terms of defining an optimal cavity *Q* (bandwidth), pulse lengths, and sample temperature, and uses a Bruker E580 system and MD4 cavity that has previously consistently given excellent results.[56]

In these comparisons, the modulation depths of the traces remain comparable as the pump pulse excites a similar fraction of spins at both frequencies, and the gain is primarily due to the larger spin echoes. Much larger increases in relative sensitivity have been observed compared to commercial *W*-band PELDOR systems (Bruker E680 with 100 mW available pulse power using a cylindrical cavity). The increased gain in sensitivity in this case is due to the much larger available excitation bandwidths for both the pump and the probe pulses as well as the use of the nonresonant sample holder where much larger volume samples more than compensate for the reduced conversion factor.

IV. DISCUSSION

It would appear that for many samples of interest, dielectric losses are sufficiently low to permit high B_1 fields and short $\pi/2$ pulse lengths in nonresonant sample holders at 94 GHz using kilowatt power levels. In conjunction with the high isolation provided by induction mode, this leads to a combination of excellent concentration sensitivity and large instantaneous bandwidth, low dead time, high spectral resolution, and orientation selectivity combined with relatively easy sample handling. These potentially open up a whole new array of experimental possibilities for pulsed EPR.

The 1 GHz instantaneous bandwidth allows ELDOR methodologies to be exploited fully, for both nitroxides and transition metals ions, which have broad spectra in high fields. It would appear that order of magnitude improvements in concentration sensitivity relative to *X*-band are possible for PELDOR measurements, potentially reducing averaging times by two orders of magnitude—an important consideration when typical measurement times can be 24 h or more. Many protein complexes are also only available at low concentrations, and low concentration levels can also be expected to substantially reduce the background intermolecular contribution. The large instantaneous bandwidth also permits full orientation dependent four pulse PELDOR measurements in which any spin orientation may be correlated with any other orientation. This has potential for characterizing conformational changes associated with angular movements between domains, even in the presence of large distance distributions.

Hyperfine techniques should also benefit from larger excitation bandwidths and better orientation selectivity. At present, HYSCORE spectroscopy is rarely used at high fields partly because nuclear Zeeman frequencies often exceed hyperfine couplings, and also because low excitation bandwidth pulses strongly limit sensitivity.[30,57] ENDOR measurements become particularly powerful at high magnetic fields due to

the clear separation of different centers with different nuclear Zeeman frequencies and higher sensitivity can be expected for Mims ENDOR relative to current commercial systems due to the larger excitation bandwidths and sample volumes. Excitation bandwidth is not so critical for Davies ENDOR but there is also potential to increase the sensitivity of such measurements by further increasing the sample volume, by increasing the transverse dimensions of the sample holder. Hyperfine strategies such as ELDOR-detected NMR can be expected to benefit from high instantaneous bandwidth and FID-detected NMR benefits from lower dead time. Low dead time is essential for the successful implementation of Fourier transform EPR, time resolved EPR, and for any spin echo measurements where the phase memory time of the system is short.

Dynamic nuclear polarization (DNP) at high fields is currently attracting considerable attention because of the very high electron polarization that may in principle be transferred to the nuclei, and spectacular enhancements in NMR sensitivity have recently been demonstrated.[58] A recent special edition of applied magnetic resonance covered recent developments.[59] Here, nonresonant techniques become particularly important as it is critical for most applications that sample volume is high enough to give good NMR filling factors. Currently, all cw polarization transfer mechanisms (Overhauser effect, solid effect, cross effect, and thermal mixing) become less efficient at high fields partly because of broadening of the spectra. In principle, however, the same methodologies should also work with pulse excitation, which may have the benefit of allowing more electron spins to contribute to the polarization process. Initial work in our laboratory has given promising results. A number of coherent polarization transfer methods using pulse techniques have also been suggested at high fields,[60] including rotating frame DNP,[61] the integrated solid effect, and the nuclear orientation via electron spin locking (NOVEL) experiment, along with optimal control strategies.[62] These potentially offer higher polarization efficiencies and most benefit significantly from larger B_1 fields, high excitation bandwidths, and flexibility in specifying complex pulse sequences.

The past few years have seen significant advances in millimeter- and submillimeter-wave technologies and we believe we have demonstrated that considerable increases in pulsed EPR performance are possible at high fields. It can be anticipated as high power and high bandwidth amplifiers are further developed over a range of frequencies that high field pulsed EPR is likely to be a very active area of research in the coming years.

ACKNOWLEDGMENTS

[1] Y. S. Lebedev, in *Electron Paramagnetic Resonance*, edited by B. C. Gilbert, N. M. Atherton, and M. J. Davies (Royal Society of Chemistry, Cambridge, 1994), Vol. 14, p. 63; A. A. Doubinskii, in *Electron Paramagnetic Resonance*, edited by N. M. Atherton, B. C. Gilbert, and M. J. Davies (Royal Society of Chemistry, Cambridge, 1998), Vol. 16, p. 211; G. M. Smith and P. C. Riedi, in *Electron Paramagnetic Resonance*, edited by N. M. Atherton, B. C. Gilbert, and M. J. Davies (Royal Society of Chemistry, Cambridge, 2000), Vol. 17, p. 164; G. M. Smith and P. C. Riedi, in *Electron Paramagnetic Resonance*, edited by B. C. Gilbert, M. J. Davies, and D. M. Murphy (Royal Society of Chemistry, Cambridge, 2002), Vol. 18, p. 254.

[2] G. R. Eaton and S. S. Eaton, Appl. Magn. Reson. **16**, 161 (1999); *Very High Frequency (VHF) ESR/EPR*, edited by O. Grinberg and L. J. Berliner (Kluwer, Dordrecht, 2004).

[3] G. M. Smith and P. C. Riedi, in *Electron Paramagnetic Resonance*, edited by B. C. Gilbert, M. J. Davies, and D. M. Murphy (Royal Society of Chemistry, Cambridge, 2004), Vol. 19, p. 338; P. C. Riedi, in *Electron Paramagnetic Resonance*, edited by B. C. Gilbert, M. J. Davies, and D. M. Murphy (Royal Society of Chemistry, Cambridge, 2006), Vol. 20, p. 245.

[4] A. I. Smirnov, in *Electron Paramagnetic Resonance*, edited by B. C. Gilbert, M. J. Davies, and D. M. Murphy (Royal Society of Chemistry, Cambridge, 2002), Vol. 18, p. 109; T. I. Smirnova and A. I. Smirnov, in *ESR Spectroscopy in Membrane Biophysics*, edited by M. A. Hemminga and L. J. Berliner (Springer, New York, 2007).

[5] K. Möbius, Chem. Soc. Rev. **29**, 129 (2000).

[6] Z. C. Liang and J. H. Freed, J. Phys. Chem. B **103**, 6384 (1999).

[7] J. H. Freed, Annu. Rev. Phys. Chem. **51**, 655 (2000).

[8] G. M. Smith, P. Cruickshank, D. R. Bolton, and D. A. Robertson, in *Electron Paramagnetic Resonance*, edited by B. C. Gilbert, M. J. Davies, and D. M. Murphy (Royal Society of Chemistry, Cambridge, 2008), Vol. 21, p. 216.

[9] K. A. Earle, D. E. Budil, and J. H. Freed, in *Advances in Magnetic and Optical Resonance*, edited by W. S. Warren (Academic, New York, 1996), Vol. 19, p. 253; K. A. Earle and J. H. Freed, Appl. Magn. Reson. **16**, 247 (1999).

[10] W. R. Hagen, Coord. Chem. Rev. **190**, 209 (1999).

[11] O. Burghaus, M. Rohrer, T. Gotzinger, M. Plato, and K. Möbius, Meas. Sci. Technol. **3**, 765 (1992); E. J. Reijerse, P. J. van dam, A. A. K. Klaasen, W. R. Hagen, P. J. M. van Bentum, and G. M. Smith, Appl. Magn. Reson. **14**, 153 (1998).

[12] P. J. van Dam, A. A. K. Klaasen, E. J. Reijerse, and W. R. Hagen, J. Magn. Reson. **130**, 140 (1998).

[13] D. Gatteschi, J. Phys. Chem. **104**, 9780 (2000).

[14] D. M. Murphy and C. C. Rowlands, Curr. Opin. Solid State Mater. Sci. **5**, 97 (2001).

[15] K. Katsumata, J. Phys.: Condens. Matter **12**, R589 (2000).

[16] M. Martinelli, C. A. Massa, L. A. Pardi, V. Bercu, and F. F. Popescu, Phys. Rev. B **67**, 014425 (2003).

[17] J. van Slageren, S. Vongtragool, B. Gorshunov, A. A. Mukhin, N. Karl, J. Krzystek, J. Tesler, A. Muller, C. Sangregorio, D. Gatteschi, and D. Dressel, Phys. Chem. Chem. Phys. **5**, 3837 (2003).

[18] A. Schweiger and G. Jeschke, *Principles of Pulse Electron Paramagnetic Resonance* (Oxford University Press, New York, 2001).

[19] T. Prisner, M. Rohrer, and F. MacMillan, Annu. Rev. Phys. Chem. **52**, 279 (2001); D. Goldfarb and D. Arieli, Annu. Rev. Biophys. Biomol. Struct. **33**, 441 (2004).

[20] K. Möbius and A. Savitsky, in *Electron Paramagnetic Resonance*, edited by B. C. Gilbert, M. J. Davies, and D. M. Murphy (Royal Society of Chemistry, Cambridge, 2008), Vol. 21.

[21] R. T. Weber, J. A. J. M. Disselhorst, L. J. Prevo, J. Schmidt, and W. T.

Wenckebach, J. Magn. Reson. **81**, 129 (1988).

[22] A. Y. Bresgunov, A. A. Dubinskii, V. Krymov, Y. G. Petrov, O. G. Poluetkov, and Y. S. Lebedev, Appl. Magn. Reson. **2**, 715 (1991).

[23] T. F. Prisner, S. Un, and R. G. Griffin, Isr. J. Chem. **32**, 357 (1992).

[24] T. Prisner, M. Rohrer, and K. Möbius, Appl. Magn. Reson. **7**, 167 (1994).

[25] D. Schmalbein, G. G. Maresch, A. Kamlowski, and P. Höfer, Appl. Magn. Reson. **16**, 185 (1999).

[26] I. Gromov, V. Krymov, P. Manikandan, D. Arieli, and D. Goldfarb, J. Magn. Reson. **139**, 8 (1999).

[27] M. Rohrer, O. Brugmann, B. Kinzer, and T. F. Prisner, Appl. Magn. Reson. **21**, 257 (2001); M. M. Hertel, V. P. Denysenkov, M. Bennati, and T. F. Prisner, Magn. Reson. Chem. **43**, S248 (2005).

[28] H. Blok, D. J. A. M. Disselhorst, S. B. Orlinskii, and J. Schmidt, J. Magn. Reson. **166**, 92 (2004); S. B. Orlinskii, H. Blok, E. J. Groenen, J. Schmidt, P. G. Baranov, C. de Mello Donega, and A. Meijerink, Magn. Reson. Chem. **43**, S140 (2005).

[29] J. W. Sidabras, R. R. Mett, W. Froncisz, T. G. Camenisch, J. R. Anderson, and J. S. Hyde, Rev. Sci. Instrum. **78**, 034701 (2007).

[30] D. Goldfarb, Y. Lipkin, A. Potapov, Y. Gorodetsky, B. Epel, A. M. Raitsimring, M. Radoul, and I. Kaminker, J. Magn. Reson. **194**, 8 (2008).

[31] W. Hofbauer, K. A. Earle, C. R. Dunnam, J. K. Moscicki, and J. H. Freed, Rev. Sci. Instrum. **75**, 1194 (2004).

[32] D. R. Bolton, P. S. Cruickshank, D. A. Robertson, and G. M. Smith, Electron. Lett. **43**, 346 (2007).

[33] D. A. Robertson, D. R. Bolton, P. A. S. Cruickshank, and G. M. Smith, *IRMMW-THz2007: Joint 32nd International Conference on Infrared and Millimeter Waves and 15th International Conference on Terahertz Electronics*, Cardiff, UK (IEEE, New York, 2007).

[34] C. H. Lee, S. Mak, and A. P. DeFonzo, Electron. Lett. **14**, 733 (1978); IEEE J. Quantum Electron. **QE-16**, 277 (1980); A. M. Vaucher, C. D. Striffler, and C. H. Lee, IEEE Trans. Microwave Theory Tech. **MTT-31**, 209 (1983).

[35] P. A. S. Cruickshank, D. A. Robertson, and G. M. Smith, *IRMMW-THz2005: Joint 30th International Conference on Infrared and Millimeter Waves and 13th International Conference on Terahertz Electronics*, Williamsburg, VA (IEEE, New York, 2005).

[36] P. F. Goldsmith, *Quasioptical Systems* (IEEE, New York, 1998).

[37] J. C. G. Lesurf, *Millimetre-Wave Optics, Devices and Systems* (Adam Hilger, Bristol, 1990).

[38] P. J. B. Clarricoats and A. D. Olver, *Corrugated Horns for Microwave Antennas* (Peter Peregrinus, London, 1984).

[39] J. A. Murphy, Int. J. Infrared Millim. Waves **8**, 1165 (1987).

[40] G. M. Smith, P. A. S. Cruickshank, D. R. Bolton, D. A. Robertson, and R. J. Wylde, *IRMMW-THz2007: Joint 32nd International Conference on Infrared and Millimeter Waves and 15th International Conference on Terahertz Electronics*, Cardiff, UK (IEEE, New York, 2007).

[41] R. I. Hunter, D. A. Robertson, P. Goy, and G. M. Smith, IEEE Trans. Microwave Theory Tech. **55**, 890 (2007).

[42] J. L. Doane, in *Infrared and Millimeter Waves*, edited by K. J. Button (Academic, New York, 1985), Vol. 13, Chap. 4.

[43] D. T. Teaney, M. P. Klein, and A. M. Portis, Rev. Sci. Instrum. **32**, 721 (1961); G. M. Smith, J. C. G. Lesurf, R. H. Mitchell, and P. C. Riedi, *ibid.* **69**, 3924 (1998); M. Fuchs, T. Prisner, and K. Möbius, *ibid.* **70**, 3681

(1999).

[44] P. Borbat, R. Crepeau, and J. H. Freed, J. Magn. Reson. **127**, 155 (1997).

[45] W. B. Lynch, K. A. Earle, and J. H. Freed, Rev. Sci. Instrum. **59**, 1345 (1988); J. Krzystek, A. Sienkiewicz, L. Pardi, and L.-C. Brunel, J. Magn. Reson. **125**, 207 (1997).

[46] G. A. Rinard, R. W. Quine, R. W. Harbridge, R. Song, G. R. Eaton, and S. S. Eaton, J. Magn. Reson. **140**, 218 (1999).

[47] P. Höfer and P. Carl, BRUKER Spin Report No. 157, 2006.

[48] A. Weber, O. Schiemann, B. Bode, and T. F. Prisner, J. Magn. Reson. **157**, 277 (2002).

[49] W. L. Hubbell, A. Gross, R. Langen, and M. A. Lietzow, Curr. Opin. Struct. Biol. **8**, 649 (1998); W. L. Hubbell, D. S. Cafiso, and C. Altenbach, Nat. Struct. Biol. **7**, 735 (2000).

[50] O. Schiemann and T. F. Prisner, Q. Rev. Biophys. **40**, 1 (2007); O. Schiemann, N. Piton, Y. Mu, G. Stock, J. W. Engels, and T. F. Prisner, J. Am. Chem. Soc. **126**, 5722 (2004); P. G. Fajer, L. Brown, and L. Song, in *ESR Spectroscopy in Membrane Biophysics*, edited by M. A. Hemminga and L. J. Berliner (Springer, New York, 2007).

[51] G. Jeschke and Y. Polyhach, Phys. Chem. Chem. Phys. **9**, 1895 (2007).

[52] M. Pannier, S. Veit, A. Godt, G. Jeschke, and H. W. Spiess, J. Magn. Reson. **142**, 331 (2000).

[53] V. P. Denysenkov, T. F. Prisner, J. Stubbe, and M. Bennati, Proc. Natl. Acad. Sci. U.S.A. **103**, 13386 (2006).

[54] V. P. Denysenkov, T. Prisner, J. Stubbe, and M. Bennati, Appl. Magn. Reson. **29**, 375 (2005).

[55] Y. Polyhach, A. Godt, C. Bauer, and G. Jeschke, J. Magn. Reson. **185**, 118 (2007).

[56] R. Ward, A. Bowman, H. El MKami, T. Owen-Hughes, and D. G. Norman, J. Am. Chem. Soc. **131**, 1348 (2009); C. W. M. Kay, H. El MKami, R. Cammack, and R. W. Evans, *ibid.* **129**, 4648 (2007); R. Ward, D. J. Keeble, H. El MKami, and D. G. Norman, ChemBioChem **8**, 1957 (2007); G. Hagelueken, W. J. Ingledew, H. Huang, B. Petrovic-Stojanovska, C. Whitfield, H. El MKami, O. Schiemann, and J. H. Naismith, Angew. Chem., Int. Ed. Engl. **48**, 2904 (2009).

[57] S. Van Doorslaer, in *Electron Paramagnetic Resonance*, edited by B. C. Gilbert, M. J. Davies, and D. M. Murphy (Royal Society of Chemistry, Cambridge, 2008), Vol. 21.

[58] J. H. Ardenkjaer-Larsen, B. Fridlund, A. Gram, G. Hansson, L. Hansson, M. H. Lerche, R. Servin, M. Thaning, and K. Golman, Proc. Natl. Acad. Sci. U.S.A. **100**, 10158 (2003).

[59] T. Prisner and W. Kockenberger, Appl. Magn. Reson. **34**, 213 (2008).

[60] T. Maly, G. T. Debelouchina, V. S. Bajaj, K. N. Hu, C. G. Joo, M. L. Mak-Jurkauskas, J. R. Sirigiri, P. C. van der Wel, J. Herzfeld, R. J. Temkin, and R. G. Griffin, J. Chem. Phys. **128**, 052211 (2008); A. B. Barnes, G. De Paepe, P. C. A. van der Wel, K. N. Hu, C. G. Joo, V. S. Bajaj, M. L. Mak-Jurkauskas, J. R. Sirigiri, J. Herzfeld, R. J. Temkin, and R. J. Griffin, Appl. Magn. Reson. **34**, 237 (2008).

[61] C. T. Farrar, D. A. Hall, G. J. Gerfen, M. Rosay, J.-H. Ardenkjær-Larsenc, and R. G. Griffin, J. Magn. Reson. **144**, 134 (2000).

[62] N. Pomplun, B. Heitmann, N. Khaneja, and S. J. Glaser, Appl. Magn. Reson. **34**, 331 (2008); I. I. Maximov, Z. Tosner, and N. C. Nielsen, J. Chem. Phys. **128**, 184505 (2008).